Phillips Matthew, Sean (Orcid ID: 0000-0001-6408-1012)

Blenkinsopp Chris (Orcid ID: 0000-0001-5784-2805)

Splinter Kristen (Orcid ID: 0000-0002-0082-8444)

Harley Mitchell, Dean (Orcid ID: 0000-0002-1329-7945)

Turner Ian, L. (Orcid ID: 0000-0001-9884-6917)

Modes of berm and beachface recovery following storm reset: observations using a continuously scanning lidar

M. S. Phillips[1], C. E. Blenkinsopp[1,2], K. D. Splinter[1], M. D. Harley[1] and I. L. Turner[1]

[1] Water Research Laboratory, School of Civil and Environmental Engineering, UNSW Australia, 110 King St, Manly Vale, NSW, 2093, Australia.
[2] Water, Environment and Infrastructure Resilience Research Unit, Department of Architecture and Civil Engineering, University of Bath, Claverton Down, Bath BA2 7AY, UK

Corresponding author: Matthew Phillips (matthew.phillips@mhl.nsw.gov.au)

Key Points:

- Tide-by-tide analysis of an entire 76-day post-storm recovery of a sandy berm and beachface reveals four key modes of profile behaviour.
- Rates of beachface volume change per tidal cycle show losses and gains on the order of several $m^3/m/day$ with intermittent berm deposition.
- Criteria found to govern behavioural modes include dimensionless fall velocity, swash exceedance of the berm crest and ocean water levels.

This article has been accepted for publication and undergone full peer review but has not been through the copyediting, typesetting, pagination and proofreading process which may lead to differences between this version and the Version of Record. Please cite this article as doi: 10.1029/2018JF004895

Abstract:

Following the rapid and destructive impacts of storm erosion, beach recovery is a key natural process of restoration, returning eroded sediment to the subaerial beach and rebuilding coastal morphology. While the effects of storm erosion have commonly been investigated, detailed studies into post-storm recovery are currently lacking. This study investigates wave-driven recovery processes of the berm and beachface on a microtidal, swash-aligned sandy beach. Following complete removal of the berm by a significant storm event, the entire 76-day rebuilding of a swash berm is analysed at the timescale of every semi-diurnal tidal cycle, utilising high resolution (5 Hz) swash and subaerial beach profile measurements from a continuously scanning fixed lidar. Tide-by-tide rates of subaerial volume change during berm recovery were most frequently observed between 1 - 2 m^3/m/day, including losses and gains on the order of several m^3/m/day, substantially larger in magnitude than the more gradual rate of net gain (0.7 m^3/m/day) observed for the entire recovery period. Patterns of berm crest formation and vertical growth were found to be primarily governed by the neap-spring tide variations in total water levels. Tide-by-tide beachface and berm volume changes were used to classify four principal behavioural modes of subaerial profile variability during recovery. Using decision tree classification, modes were differentiated according to nearshore dimensionless fall velocity, swash exceedance of the berm crest and ocean water levels. The findings provide novel behavioural and parametric insight into the tide-by-tide rebuilding of the beachface and berm by swash throughout a complete post-storm recovery period.

1. Introduction

Understanding the dynamic nature of beaches is critical to managing densely populated and asset-rich coastal regions (Bascom, 1954). Counter-acting the destructive impact of storms is the onshore return of eroded sediment and associated post-storm rebuilding of the subaerial beach (i.e., the beachface, berm and dunes) due to the action of waves and wind. This post-storm rebuilding process is often referred to in the literature as ‘beach recovery’ (e.g., Morton et al., 1994; Corbella & Stretch, 2012). As a beach recovers, the depleted post-storm buffer provided by the subaerial beach that protects adjacent coastal settlement and infrastructure from coastal inundation is progressively restored in width, volume and height (CERC, 1984). Additionally, during recovery the “usable” width of a beach is restored to satisfy beach goers (Frampton, 2010) and impacted beach ecology returns to its former state of health (Revell et al., 2011). While studies have developed empirical and process-based understanding of storm erosion (e.g., Larson & Kraus, 1989; Roelvink et al., 2009), insight

into beach recovery and the physical parameters governing the rebuilding of subaerial beach profile are less well observed and understood (e.g., Jensen et al., 2009; Corbella & Stretch, 2012; Burvingt et al., 2018; Dodet et al., 2018).

After wave action has transported sediment from the nearshore to the shoreline during post-storm beach recovery (Phillips et al., 2017), swash processes then rework inter-tidal zone sediment up onto the subaerial beach to rebuild the berm. The sandy beach berm is characterised by a near-planar region of the subaerial beach, extending seaward of the foredune toe and separated from the steeper beachface often by a distinctive change in gradient, known as the berm crest (Masselink & Hughes, 2003). The rebuilding of the berm and beachface by swash processes marks the most landward extent of wave-driven processes during beach recovery, beyond which more gradual aeolian processes rebuild eroded morphology in the backshore and dunes (Morton et al., 1994). The majority of previous investigations of swash-driven beachface (i.e., seawards of the berm crest and extending to mean sea level, MSL) and berm (i.e., landwards of the berm crest and seawards of the foredune toe) morphodynamics during recovery are limited by the temporal resolution of post-storm morphology datasets which typically capture morphological and volumetric changes during recovery at monthly to yearly timescales (e.g., Morton et al., 1994; Corbella & Stretch, 2012; Kobayashi & Jung, 2012; Yu et al., 2013; Houser et al., 2015; Scott et al., 2016; Castelle et al., 2017; Burvingt et al., 2018).

Fewer studies have observed post-storm recovery at finer temporal resolutions (i.e. sub-daily), spanning weeks to months to examine beachface and berm morphodynamics associated with wave, swash and ocean water level hydrodynamics (e.g., Dubois, 1988; Katoh & Yanagishima, 1992; Austin & Masselink, 2006). Using daily beach profile measurements during the initial four months following a storm, Dubois (1988) observed two main behavioural modes in profile variability, namely the progradation (seaward growth) of the beachface and aggradation (vertical growth) of the berm. Though the reported study did not include simultaneous swash measurements, swash exceedance of the berm crest was inferred to be a likely primary factor distinguishing these two modes. Similar findings were later observed by swash measurement campaigns of berm regrowth following coastal lagoon openings, demonstrating the importance of swash exceedance above the elevation of the berm crest (Weir et al., 2006; Baldock et al., 2008). These and additional studies have provided valuable insight into smaller-scale (swash-by-swash to tide cycle) swash zone processes and morphodynamics over relatively shorter monitoring durations of days to a few weeks (e.g., Austin & Masselink, 2006; Jensen et al., 2009; Russell et al., 2009; Blenkinsopp et al., 2011). However, there remains a knowledge gap to better understand the role of

swash zone processes in the longer-term context of complete berm recovery following significant storm events (Puleo & Torres-Freyermuth, 2016).

The aim of this study is to classify and evaluate parameters governing berm and beachface morphodynamics at the timescale of individual tides throughout the complete recovery of a berm, following a significant storm event in which the berm was completely 'reset' (i.e., removed of all previous berm morphology). To do so, this study uses a continuously scanning lidar, mounted on the rooftop of a beachside building to obtain continuous and high frequency (5Hz) subaerial beach profile and swash measurements throughout the entire 2.5-month recovery period of the berm from its reset form to pre-storm state. Methodology including lidar monitoring setup and data processing is described in Section 2. Patterns of berm crest growth, rates of subaerial volume change and behavioural modes of subaerial profile variability are analysed at timesteps of each and every tidal cycle throughout berm recovery with results presented in Section 3. Using a decision tree classification, behavioural modes of berm and beachface recovery following storm reset are characterised, presented and discussed in Section 4. Key findings and conclusions are summarised in Section 5.

2. Methodology

2.1. Study site

Narrabeen-Collaroy Beach, shown in Figure 1a, is a 3.6 km-long embayed, swash-aligned, sandy beach situated on the wave-dominated SE Australian coastline. Beaches in the region were deposited during the mid-Holocene, approximately 6500 years ago, as rising sea levels began to stabilise to present-day level (Roy et al., 1980; Thom, 1984). During this period, continental shelf marine sands were transported onshore and deposited in embayments between rocky protrusions of headlands and cliffs. Many of these deposits formed barrier beaches backed by estuaries that have progressively infilled with fluvial sediments. Offshore, the coastline has a steep and narrow (20 - 70 km) continental shelf (Short & Trenaman, 1992). Waves are predominantly from the SSE direction with an average deepwater significant wave height (H_s) of 1.6 m and peak wave period (T_p) of 10 s. Semi-diurnal tides in the region are characterised by mean spring and neap ranges of 1.3 m and 0.8 m, respectively (Couriel et al., 2012).

Continuous lidar monitoring was undertaken at a single beach transect approximately 700 m north of the southern (Collaroy) extremity of the embayment. The monitoring location is partially sheltered from the predominant SSE wave energy, with nearshore H_s averaging 0.8 m at the 10 m depth contour and an average breaker wave direction of ~2.9° relative to the

shoreline orientation. Beach morphology in this region of the embayment is typically of the Low Tide Terrace (LTT) beach state (Wright and Short, 1984). The analyses presented here focus on wave-driven sediment exchanges between the subaerial and subaqueous beach (i.e. swash zone). These sediment exchanges are predominately controlled by cross-shore processes at this swash-aligned embayed beach, which have been shown at this site to be the dominant mode of shoreline variability at timescales of days to months as is the focus of this study (Davidson et al., 2013; Harley et al., 2015). For a more detailed site description of Narrabeen-Collaroy Beach the reader is referred to Turner et al. (2016).

2.2. Fixed lidar monitoring setup

Since May 2014 a near-infrared, extended-range lidar (*SICK LD-LRS 2110*) has been continuously operating from the rooftop of a beachside building at Narrabeen-Collaroy, with the instrument located approximately 44 m above mean sea level (MSL) as shown in Figure 1b. This fixed lidar deployment at Narrabeen-Collaroy operates by emitting a pulse of light that is reflected from the surface of the beach, swash and surf zone, and returned to the instrument to be recorded as a distance based on travel time. Measurements are recorded at 0.25º angular increments along a cross-shore transect, resulting in cross-shore resolutions of approximately 0.2 - 0.5 m on the subaerial beach, and 0.5 - 2 m within the surf zone. The lidar swath extends from the base of the building to the offshore limit of signal return (Figure 1b). This offshore limit is observed to vary with the degree of surf zone aeration required to obtain sufficient signal reflection from the water surface (Blenkinsopp et al., 2010). The typical scanning range of the instrument in this setting is between 70 - 110 m with a maximum range of the order of 130 m (~120 m cross-shore) during high surf zone aeration. Continuous scanning is undertaken at a frequency of 5 Hz, with brief and infrequent outages of up to a few days due to local computer issues at the field site. The fixed lidar system enables continuous 24 hours per day monitoring, with uninterrupted and identical data collection during both day and night (see Figure 3). The system is designed as shown in Figure 1b to allow remote user operation of the lidar, scan scheduling and automated online data transfer. Lower-elevation and shorter-term (days) lidar deployments for the measurement of swash and subaerial morphology are also reported in the literature (e.g., Blenkinsopp et al., 2010; Brodie et al., 2012).

Co-located with the fixed lidar is an Argus coastal imaging system (Holman and Stanley, 2007) that has been recording oblique images of the southern end of the embayment every daylight hour since August 2004 (Splinter et al., 2018). These images are used in this study to relate subaerial observations from the lidar to subaqueous changes identified in the Argus plan view timex images (Phillips et al., 2017).

2.3. April 2015 storm and post-storm recovery analysis

The purpose of this contribution is to document the complete recovery of the subaerial berm and beachface following a storm reset event. Over the 4-year period that the lidar has been continuously scanning, one such event has occurred. Between April 20 and 22, 2015, the study region was impacted by an intense extratropical cyclone referred to in this region as an 'East Coast Low' (ECL). Hourly deepwater wave buoy data acquired 11 km offshore of the study site (Figure 1a) recorded a peak significant wave height (H_s) of 8.1 m during the storm, corresponding to a 20-year deepwater H_s annual recurrence interval (Shand et al., 2010). The storm approached the coast from an average SSE (161 °TN) direction and coincided with spring high tides (maximum ocean water level = 1.22 m above mean sea level). The impact of the storm was significant, identified as the fourth most erosive storm event on record in the last 40 years of routine monitoring (1976 - 2016) at Narrabeen-Collaroy Beach (Harley et al., 2016; Harley et al., 2017). Data from the continuously scanning lidar captured both the impact of this significant erosion event, including the full erosion of the subaerial berm, as well as the complete recovery of the subaerial beach to pre-storm conditions in the 2.5 months following.

2.4. Subaerial beach profile data extraction

Subaerial beach profile variability at the lidar transect was analysed at tidal intervals (i.e., low tide to low tide) throughout the entire recovery of berm morphology following the April 2015 ECL storm event. For each low-tide, subaerial beach profiles were calculated using a 30-minute subsample of the continuous lidar dataset (5 Hz) centred about each low tide, as shown in Figure 2. Pre-processing of the raw data to obtain detailed subaerial profile (and swash zone) information required several steps. First, raw distance data relative to the fixed location of the lidar were transformed from polar to Cartesian (cross-shore distance and elevation) coordinates. Based on RTK-GPS ground control surveys of the measured transect, elevations were then converted to the local Australian Height Datum (m AHD, equivalent to mean sea level) and cross-shore distance (m) relative to a fixed landward benchmark. Elevation data were then linearly interpolated to regular 0.5 m cross-shore intervals. For every 30-minute subsample at semi-diurnal low tides, the beach profile was determined by the minimum elevation at each cross-shore interval in order to extract the sand surface extending down into the swash zone as shown in Figure 2. As the final step to distinguish the seaward limit of the measured beachface from the lower swash zone water surface, the seaward limit of the profile was defined as the minimum run down of the swash edge (refer Section 2.5 for details) that was then checked and verified by manual inspection. Comparisons with RTK-GPS profile surveys undertaken approximately each month

throughout 2015 (12 surveys in total) found that the vertical root-mean-square error of the lidar-measured profiles was 0.04 m relative to (and within the accuracy of) the RTK-GPS-measured profiles.

Using these profile data obtained at every low tide, subaerial sand volume (m^3/m) was calculated as the integrated profile area above the elevation of mean sea level (0 m above MSL), extending landward to the fixed cross-shore origin. Rates of subaerial volume change, *dv/dt* ($m^3/m/day$), between consecutive low tides measurements, *i*, were calculated as,

$$\frac{\boldsymbol{dv}}{\boldsymbol{dt}} = \frac{Volume_{i+1} - Volume_i}{Time_{i+1} - Time_i} \quad (1)$$

The position (cross-shore and elevation) of berm crests on the beach profile as shown in Figure 2 were extracted in a two-step process. First, potential berm crests were manually identified via visual inspection of the beach profile. Second, within a specified cross-shore region (±3 m) of each manually identified berm crest, the point of maximum change in the profile gradient was calculated where a flattening occurred in the landward direction. Where the corresponding change in profile gradient exceeded a threshold of 0.05, the point of maximum change in profile gradient was recorded as the position of the berm crest. As shown in Figures 2 and 3, where two or more berm crests were present, the most seaward of these features was identified as the 'primary crest', to distinguish this from the more landward 'secondary crest'. The beachface is specifically defined in this study as the region between the primary berm crest and MSL, whereas the berm is defined as the region landward of the primary berm crest. Rates of volume change in cross-shore subsections seaward (i.e. beachface, dv_{bf}/dt) and landward of the primary berm crest (i.e. berm, dv_{bm}/dt) were also calculated.

2.5. Swash and total water level data extraction

Swash water surface elevation data throughout the analysed recovery period were also obtained by the fixed lidar monitoring system. The time-varying leading edge of the swash, as shown in Figure 3, was extracted by applying a threshold technique as described by Turner et al. (2008), to the rate of change between two successive lidar scans. First, the dataset was smoothed using a running median filter (2 seconds) to reduce inherent noise (±0.03 m) in individual lidar cross-shore point measurements. Second, the rate of change of the detected lidar surface (water or bed) was calculated at each cross-shore interval between successive lidar scans. A threshold gradient of 0.02 m/s was found to effectively distinguish the stationary bed measurements (≤ 0.02 m/s) from non-stationary water surface measurements (> 0.02 m/s). The leading edge of the swash for each scan was then defined as the point of transition between bed and water surface measurements, sampled at 5 Hz.

The time series of the swash edge was referenced to the measured ocean water levels (OWL) to give the wave runup time series throughout the recovery period.

Swash statistics were analysed for each semi-diurnal (approx. 12.4 hours) tidal cycle between consecutive low tides. The time series of the swash edge was used to calculate the percentage of wave runup events exceeding the primary berm crest elevation (i.e., 'swash exceedance') for each tidal cycle. Additionally, the 2% exceedance elevation of wave runup events $R_{2\%}$ for each tidal cycle was calculated.

The total water level (TWL) for each tidal cycle is then given by,

$$TWL = R_{2\%} + OWL_{max} \quad (2)$$

where OWL_{max} was the maximum measured ocean water level (OWL) for each tidal cycle. Ocean water levels were measured every 15 minutes at the HMAS Penguin tide gauge in Port Jackson, Sydney, approximately 12 km south of the study site.

Hourly deepwater wave data H_s, T_p and θ, were acquired from the Sydney waverider buoy (Figure 1a) during the April 2015 storm and subsequent recovery. These measurements were transformed using a MIKE21 spectral wave model (DHI, 2014) to the 10 m depth contour in the nearshore directly offshore of the fixed lidar monitoring system (Mortlock & Goodwin, 2016).

The dimensionless fall velocity, Ω (Gourlay, 1968; Dean, 1973) is a common parameter used to empirically classify sediment transport direction (Larson & Kraus, 1989) and beach morphological states (Wright & Short, 1984). Dimensionless fall velocity in this study was quantified at the 10 m depth contour as,

$$\Omega = \frac{H_S}{wT_P} \quad (3)$$

where w is the fall velocity (m/s) of the beach sediment. Other nearshore wave parameters were explored in Phillips et al. (2017), including wave steepness (H/L), and disequilibrium dimensionless fall velocity (Davidson et al., 2013). Dimensionless fall velocity was shown to be significantly correlated to shoreline dynamics when the bar was semi-attached and attached to the beachface, the two phases of recovery that elicit landward sediment transport from the surf zone to the beachface, as is the focus of this study.

3. Results

3.1. Lidar observations: April 2015 storm and post-storm recovery

During the April 2015 storm, modelled nearshore H_s at the 10 m depth contour of the lidar monitoring profile is shown in Figure 4a to have peaked at 3.7 m. This is equivalent to 46% of the peak deepwater significant wave height recorded during this storm, highlighting the sheltering effect of SSE waves at this section of the embayment. The arrival of the storm coincided with spring high tides and resulted in lidar-recorded total water levels (Eq. 2) of up to 3.7 m above MSL (Figure 6a). The resulting impact on pre-storm berm and convex morphology at the lidar profile is shown in Figure 4d. Unique in the 4-year monitoring period, during the storm, the berm was completely removed, leaving a dissipative, concave post-storm subaerial profile, with minimal observed change in the foredune. This corresponded to rapid subaerial volume erosion of 55 m^3/m at the lidar profile (Figure 4b). Approximately 56% of this erosion (31 m^3/m) was observed during the first tidal cycle (approximately first 12 hours) following the onset of storm wave conditions. Similar subaerial erosion observations within the broader embayment during the event were reported by Harley et al. (2016), noting an alongshore-averaged loss of 58 m^3/m, of which over 90% was primarily from the berm and beachface below the 3 m elevation contour.

In the 2.5 months following the storm, wave conditions shown in Figure 4a were predominantly mild, with 70% of nearshore H_s below the 12-year site mean of ~0.8 m, intermittently punctuated with moderate wave events (H_s > 1 m) typically spanning a few days. The mean H_s for this entire recovery period was 0.7 m. Nearshore Ω was also predominantly mild during this period, with approximately 80% of observations less than the 12-year site mean ($\bar{\Omega} \approx 2.0$), indicative of generally mild wave energy and accretionary beach conditions. Additional wave refraction between the 10 m depth contour (Figure 4a) and the breakpoint was modelled using the nearshore wave model described in Harley et al. (2011). These results (not shown) found that the incident wave angle at the breakpoint relative to the shoreline orientation (~74° TN) over the recovery period was only 2.7° northwards on average, highlighting the overwhelmingly swash-aligned nature of the study site.

By July 7, 2015, 76 days after the storm, berm and convex profile morphology closely matching pre-storm conditions were observed (Figure 4d), and virtually all (51 m^3/m) of the eroded sand volume had returned to the subaerial beach (Figure 4b). Tide-by-tide subaerial volume and beach profile evolution captured by the lidar during this recovery period are shown in Figures 4b and 4c, respectively. Spanning the full 76-day recovery period, subaerial volume returned at a net rate of ~0.7 m^3/m/day, with moderate wave events

causing minor intermittent erosion as the beach progressively recovered. The images in Figure 5 show onshore sandbar migration that occurred concurrently throughout the 76-day berm recovery period. For the first 1.5 months (days 0 to 45 of the recovery period) the net rate of subaerial volume recovery was more gradual (~0.4 m^3/m/day) as sand predominately migrated onshore in the form of nearshore sandbars (Figure 5). In the final month (days 45 to 76), recovery of the beachface and berm progressed more rapidly (net rate of ~1.1 m^3/m/day) as nearshore sandbar morphology attached and welded to the beachface (Figure 5, discussed later in Section 3.4). Using approximately 10 years of daily image-derived shoreline data from the Narrabeen coastal imaging station, Phillips et al. (2017) found similar temporal variability and rates in shoreline recovery/beach face accretion following historical storm activity and linked these rates to the proximity of sandbars with respect to the shoreline.

3.2. Berm crest formation and growth during recovery

The time series of ocean water level (OWL), total water level (TWL) and berm crest elevation throughout the recovery period are shown in Figure 6a. A close relationship is observed between the formation and vertical growth of the primary berm crest during recovery with neap-spring variations in total water level. This was particularly apparent in the later stages of the recovery period (days 30 and onwards). The formation of a new berm crest on lower regions of the beach profile was observed during neap tides, i.e., a neap berm (e.g., days 33 to 35, Figure 6a). During subsequent 7-day periods of neap to spring tides (that occur approximately twice per month) and rising TWL, the berm crest underwent vertical growth (e.g., days 35 to 42). For these time periods, the increasing berm crest elevation significantly correlated to the rising TWL ($R = 0.94$, $P<0.0001$), as the TWL extended higher up the beachface. Rates of vertical berm crest growth during these periods were found to be similarly significantly correlated ($R = 0.82$, $P<0.0001$) to the swash exceedance of the berm crest per tidal cycle (Figure 6b). The observed vertical growth of the berm crest then ceased during spring tides (e.g., days 42 to 43) at the maximum TWL. The TWL then decreased in elevation during spring to neap tides (e.g., days 43 to 50), stranding the berm crest and confining swash deposition to the beachface. At the subsequent neap tide, this deposition was typically observed to form a new primary berm crest, seaward of the prior and now secondary berm crest; with this cycle reoccurring throughout the remainder of the recovery period.

3.3. Rates of subaerial volume change during recovery

Figure 7a summarises the frequency distribution of observed rates of tide-by-tide (i.e., approximately every ~12 hours) subaerial volume change throughout the entire 76-day

recovery period. The distribution is found to be unimodal with a positive peak at 1 - 2 m^3/m/day and slightly negatively skewed. Considerable variability is revealed in these rates of subaerial volume change observed at tidal intervals (s.d. = 3.1 m^3/m/day), including the occurrence of gains (positive) and losses (negative) of sand of the order of several m^3/m/day, with magnitudes up to several orders larger than the observed and more gradual net rate of underlying recovery (approximately 0.7 m^3/m/day). This indicates that during beach recovery and predominantly mild wave conditions, significant fluctuations (positive and negative) in rates of subaerial beach volume change can take place at the timescale of individual tides.

Figures 6b and 6c separate the respective distributions of beachface and berm volume changes during the same recovery period. The similarity of distributions in Figures 6a and 6b indicate that observed variability in measured rates of subaerial volume changes occurred predominantly on the beachface (s.d. 3.0 m^3/m/day). In comparison, more uniform and gradual deposition (s.d. = 0.71 m^3/m/day, most commonly 0 - 1 m^3/m/day,) was observed on the berm with periods of no volume change when the TWL was below the primary berm crest (Figure 7c). Figure 7d shows the cumulative volume changes for the beachface and berm over the recovery period. Berm deposition in Figure 7d occurred intermittently throughout the 76-day recovery period, when swash exceeded the berm crest. By the end of this full recovery period, beachface and berm deposition accounted for 59% and 41%, respectively, of the volume returned to the subaerial beach.

3.4. Modes of profile variability during berm and beachface recovery

To begin to synthesize and characterise the observations and analyses presented above, Figure 8 compares rates of daily beachface volume change to the corresponding berm volume change, spanning the entire 76-day recovery period. This figure reveals that the observations can be usefully separated into four different behavioural modes of berm and beachface recovery. To assist the interpretation of these four distinct recovery modes, example phases when each was dominant are shown in Figure 8b. These four modes are separately described and interpreted below.

Mode 1: Beachface progradation

Beachface progradation (Mode 1, shown in green in Figure 8) was the most frequently observed mode during the recovery period, accounting for nearly half (47%) of the observations. During this mode, sediment is transported from the inner surf zone to the lower beachface, causing a seaward growth of the beachface with no berm deposition. In some cases (e.g. days 45 to 53), this coincided with the welding of sandbars to the lower

beachface, leading to rapid shoreline advancement (as shown in Figure 8b, green and Figure 5). Tide-by-tide rates of subaerial volume change during beachface progradation averaged 2.0 m^3/m/day (s.d. = 1.3 m^3/m/day) and reached up to 6.9 m^3/m/day on day 32 following minor beachface erosion that was observed to rapidly return onshore. Beachface progradation often led to the formation of a new neap berm crest as seen during days 59 to 65 of recovery in Figure 9.

Mode 2: Beachface progradation with berm aggradation

The second most frequent (22% of observations) mode of profile change during recovery was beachface progradation with berm aggradation (Mode 2, red in Figure 8). This mode involves the seaward growth of the upper beachface and vertical growth of the berm (Figure 8b, red), with sediment transport from the inner surf zone and lower beachface. Daily rates of subaerial volume change averaged 2.3 m^3/m/day (s.d. = 1.6 m^3/m/day). For Mode 2, the deposition was observed higher up the beach profile than for mode 1 and led to the vertical growth of the berm crest with rates averaging 0.10 m/day (s.d. = 0.15 m/day). When this second mode was observed to persist over several days, the beachface steepened about a nodal-point on the lower profile, as seen in Figure 9. In the final weeks of recovery from day 65 onwards (Figure 9), mode 2 was particularly prevalent. This led to a significant vertical growth by 1.5 m of a newly formed berm crest due to overwash deposition. During this aggradation of the berm, the intertidal zone gradually steepened by a factor of three, reinforcing higher wave runup and overwash deposition. This rapid steepening indicates an exhausting of intertidal sandbar welding capacity and reduction in sediment feed from the inner nearshore toward the completion of the post-storm recovery period.

Mode 3: Berm aggradation with beachface erosion

Observed slightly less frequently (15% of observations) throughout the total recovery period was berm aggradation coinciding with beachface erosion (Mode 3, light blue in Figure 8). During Mode 3, sediment is transported from the beachface and deposited on the berm and lower intertidal zone. This third mode of beachface/berm behaviour was found to lead to beachface concavity (Figure 8b, light blue) and typically resulted in a net loss of sediment from the subaerial beach, with rates averaging -1.8 m^3/m/day (s.d. = 2.3 m^3/m/day). Rapid vertical berm growth was also observed, averaging 0.29 m/day (s.d. = 0.18 m/day) and reaching up to 0.58 m/day. In Figure 8a, the growth of the berm was almost only observed with some degree of change to the beachface, whether progradation (Mode 2) or erosion (Mode 3). This is not surprising considering sediment must first be transported across the beachface prior to deposition on the berm and some degree of beachface deposition or erosion is likely in this active region of the profile.

Mode 4: Beachface erosion without berm aggradation

Beachface erosion without berm aggradation (Mode 4, dark blue in Figure 8) was also observed (15% of observations). This involves the offshore transport of sediment from the subaerial beach to the inner surf zone, here observed at an average rate of -1.9 m^3/m/day (s.d. = 2.0 m^3/m/day).

Though not shown in Figure 8, an additional and less common mode of profile change was also observed, accounting for less than 1% of all observations (day 11 only) during the recovery period. This corresponded to the removal of a neap-tide berm deposit, temporarily resetting morphology to prior post-storm conditions. Though infrequent, this mode led to rapid changes with an observed rate of subaerial volume change of -15 m^3/m/day; -10 m^3/m/day on the beachface and -4.6 m^3/m/day on the berm, respectively.

4. Discussion

Following the complete resetting of the berm and beachface morphology by a significant storm event, the present findings provide detailed observations and insight into the nature and characteristics of subaerial beach recovery, through the use of a fixed and continuous scanning lidar to quantify at high spatial and temporal resolution the complete return of the subaerial profile to its pre-storm configuration. When observed at the timescale of each and every semi-diurnal tide, a high degree of variability is revealed in rates of subaerial volume change throughout the observed 76-day recovery period (Figure 7a), including losses and gains of the order of several m^3/m/day, substantially larger in magnitude than the more gradual rate of net gain for the entire recovery period (here observed at 0.7 m^3/m/day). Importantly, this shows that during beach recovery following a storm (most often considered a period characterised by gradual accumulation of sand volume), significant fluctuations (positive and negative) in rates of subaerial beach volume change can take place. These new data obtained at high temporal resolution show that erosion, as well as deposition, may occur on the timescale of individual tides during berm and beachface recovery, and that these rates can be several orders of magnitude larger than the observed and more gradual net rate (observed here to be approximately 0.7 m^3/m/day) of underlying recovery.

Similar results were observed by Phillips et al. (2017), highlighting fortnightly and weekly variability in rates of shoreline recovery, related to different sandbar and nearshore wave conditions. Specifically, the highest rates of shoreline recovery were linked to bar-welding events, whereby sand in the surf zone was transport landward by swash processes onto the lower beachface. The new tide-by-tide observations presented in this study are also

comparable to previous studies that have measured similar distributions of beachface/berm variability at sub-tidal (Russell et al., 2009) and swash-by-swash (Turner et al., 2008; Blenkinsopp et al., 2011) timescales, though for much shorter durations than the entire 76-day recovery period presented here. The variability of the subaerial beach is noted when observed at finer (sub-daily) temporal resolutions; constantly changing and being reshaped by swash activity. It is the integrated effect of this shorter-term variability characterised by rates of significant magnitude in both directions, which underlies the overall and much more gradual net recovery of the subaerial beach with time.

Figures 6b-c show that the majority of variability in rates of subaerial volume change occur at the beachface in the lower swash, with more gradual and intermittent growth on the berm in the upper swash zone. These results are consistent with detailed studies of swash zone sediment flux distributions (Baldock et al., 2006; Blenkinsopp et al., 2011), which show that the largest cross-shore sediment fluxes are typically observed in the low to mid swash zone, leading to greater morphological variability. In the upper swash zone where the berm forms, cross-shore sediment fluxes are generally smaller and favour the deposition of suspended sediment due to small/decelerating uprush velocities and low backwash velocities (Blenkinsopp et al., 2011). This effect is enhanced by the planar or slightly landward slope of the berm in the upper swash that with swash exceedance of the berm crest, acts as a region of infiltration and deposition with low backwash acceleration. In the present study, the intermittent growth of the berm was found to involve a repeated cycle of berm crest formation and vertical growth in conjunction with neap-spring tide variations in total water levels. Similar neap-spring tide patterns of berm crest formation and growth were also observed by Hine (1979) along a migrating barrier spit at Nauset Beach, United States.

4.1. Behavioural modes of berm recovery

Behavioural modes describing the recovery of berm and beachface morphology following removal by a storm have previously been reported by Dubois (1988). This earlier study identified two modes of beach recovery: beachface progradation (seaward) and berm aggradation (vertical) with upper beachface deposition, corresponding to Modes 1 and 2 identified in the present study (Figure 8a). Dubois (1988) reported these two more general modes of beachface and berm response to occur in sequential stages, where berm aggradation (vertical growth) was predominant in the initial months following a storm and later followed by beachface progradation (seaward growth) once swash no longer exceeded an established berm crest. Following a lagoon entrance opening, Weir et al. (2006) also noted similar modes of berm growth, particularly during spring (neap) tides when swash exceedance conditions were present (absent).

The new and detailed tide-by-tide observations presented here of the entire recovery of a berm following complete removal by a significant storm, extends this prior work by distinguishing and characterising in greater detail the morphodynamics and related forcing of berm recovery. This includes the identification of four distinct modes of berm recovery including two modes of berm aggradation with differing beachface responses (Modes 2 and 3) as well as the observation of beachface erosion without berm aggradation (Mode 4) during recovery. Figure 10a shows the time series of the four behavioural modes identified in this study, overlayed on the return of subaerial volume throughout the entire 76-day recovery period examined here. This figure shows phases when certain modes are prevalent (e.g., Mode 1 on day 45 - 53 and Mode 2 on day 33 - 38), as well as phases of high tide-by-tide variability between modes (e.g., day 53 - 60).

An extensive range of nearshore wave, swash, ocean water level and morphological forcing parameters were explored for their ability to distinguish conditions associated with these different modes. Based on the decision tree classification presented graphically in Figure 10e, differentiation of each of the four recovery modes is best achieved based on the dimensionless fall velocity Ω (Figure 10b), swash exceedance of the berm crest (Figure 10c) and ocean water level (Figure 10d).

Referring to Figure 10b, the value of $\bar{\Omega}$ (≈ 2.0) is defined as the long-term (12-year) site mean dimensionless fall velocity. The primary differentiator was dimensionless fall velocity Ω, with branches for mild ($\Omega < \bar{\Omega}$), moderate ($\Omega > \bar{\Omega}$ and non-storm conditions) and high (storm conditions where H_s was above the 5% exceedance level for a minimum duration of one tidal cycle. During these conditions Ω in excess of 4 was observed).

Following down the branch of mild wave conditions ($\Omega < \bar{\Omega}$) in Figure 10e, the next defining condition was the presence/absence of swash exceedance of the berm crest. With no swash exceedance of the berm crest (Figure 10c) beachface progradation (Mode 1) was most frequently observed (86%). Phases of several days of Mode 1 beachface/berm behaviour and no swash exceedance are seen in Figures 9a and 9c, respectively. This mode of recovery typically occurred as the tide range declined from spring to neap (Figure 10d) resulting in the TWL generally not reaching the elevation of the berm crest (Figure 6a). Under these conditions, deposition in the upper swash zone was concentrated on the beachface, while surf/swash boundary processes acting lower on the beach profile likely enhanced suspended sediment transport from the inner surf zone (Blenkinsopp et al., 2011). Berm crest formation, often observed following Mode 1 (as in Figure 9), may perhaps be initiated by reduced tidal shifting of swash zone processes across the beachface at neap tides, concentrating deposition at a constant elevation in the upper swash.

The left-hand branches of the decision tree in Figure 10e show conditions of mild waves ($\Omega < \bar{\Omega}$) and swash exceedance of the berm crest, for which berm aggradation Modes 2 and 3 were most frequently observed. In particular, during lower ocean water levels (OWL < MHWS) on the far-left branch of the decision tree, 77% of observations were berm aggradation with beachface progradation (Mode 2). In Figure 10a, phases of several days of Mode 2 are observed (e.g., days 34 -38, 65 - 69), coinciding with neap-spring tides and rising total water levels after new berm crest formation (Figure 10d). With these conditions, upper swash zone deposition was observed to move slightly up the beachface and onto the berm, while lower swash zone processes are seen to remove sediment from the lower beachface (Figure 10e). This also explains the observed steepening of the beachface about a null-point on the lower profile during this mode (Figure 9), also noted by Dubois (1988). In Figure 10a, the occurrence of Mode 2 was observed to become more intermittent with the onset of spring tides (e.g., day 69 - 73), when occurring during the smaller semi-diurnal high tide.

On the left-hand branch shown in Figure 10e, with mild wave conditions ($\Omega < \bar{\Omega}$), swash exceedance of the berm crest and spring tide ocean water levels (OWL > MHWS), beachface erosion with berm aggradation (Mode 3) was the predominant response observed (66% of observations). Interestingly, subaerial volume changes during this response indicated net offshore sediment transport, even with mild waves. This is perhaps due to more energetic lower swash zone processes shifting higher up the beachface with spring high tides, such that the majority of the beachface becomes a source of sediment. Some of this sediment is observed to be deposited on the berm via swash exceedance of the berm crest, however is predominantly transported offshore to the inner-surf zone. Reduced wave-breaking during larger high tides due to increased surf zone water depths may enhance this effect, increasing incident wave energy and sediment transport at the beachface (Guedes et al., 2011).

The middle branches of Figure 10e decision tree show the most prevalent modes with moderate wave conditions ($\Omega > \bar{\Omega}$ and *non-storm*) during recovery. In particular, with moderate waves and lower ocean water levels (OWL< MHWS), beachface progradation (Mode 1) was again observed to be the predominant response (77% of observations). However, with moderate waves and higher ocean water levels (OWL > MHWS), beachface erosion without berm aggradation (Mode 4) was most frequently observed (58% of observations). Similar to conditions with mild waves and swash exceedance, ocean water levels are again observed to be a key factor differentiating modes associated with beachface progradation and erosion at the timescale of individual tides. These results suggest the

importance of tidal variations in ocean water levels shifting inner surf zone and swash zone processes to drive variability in tide-by-tide rates of volume change and profile configuration at the beachface throughout recovery.

Finally, the far-right branch of the decision tree in Figure 10e indicates the temporary resetting of the berm when intermediate storm wave conditions occurred during the recovery period on day 11. The occurrence of intermediate storm erosion during recovery is a common observation on high-energy coastlines (e.g., Corbella & Stretch, 2012; Scott et al., 2016; Phillips et al., 2017). Though not observed in the present recovery period, it is noted that minor storms can also result in the formation of a higher and narrower storm berm in the beach profile (Psuty, 1965; Morton et al., 1994). While intermediate storms may lead to temporary erosion of the subaerial beach during recovery, further research is warranted into the effect of higher wave energy on the subaqueous beach during recovery, potentially transporting storm deposits in deeper waters onshore (Scott et al., 2016; Castelle et al., 2017; Burvingt et al., 2018).

5. Conclusion

Tide-by-tide swash and subaerial beach profile observations obtained from a continuously scanning lidar at Narrabeen-Collaroy Beach, Australia, were used to analyse beachface and berm morphodynamics throughout a complete (~2.5 month) recovery of berm morphology following removal by a significant storm event. Tide-by-tide rates of subaerial volume change during berm recovery were most frequently between 1 - 2 m^3/m/day, including losses and gains on the order of several m^3/m/day, substantially larger in magnitude than the more gradual rate of net gain (0.7 m^3/m/day) observed for the entire recovery period.

Patterns of berm crest formation and vertical growth were observed to be primarily governed by the neap-spring tide variations in total water levels. In particular, rates of volume change were most variable on the beachface but were more gradual and intermittent on the berm. Beachface and berm volume changes observed at every semi-diurnal tide reveal four principal behavioural modes of subaerial profile variability during berm recovery; beachface progradation (Mode 1), beachface progradation with berm aggradation (Mode 2), beachface erosion with berm aggradation (Mode 3) and beachface erosion without berm aggradation (Mode 4). Based on a decision tree classification, these primary modes of beach and berm adjustment can be differentiated by nearshore dimensionless fall velocity, swash exceedance of the berm crest and ocean water level. These findings provide new behavioural and parametric insight into the tide-by-tide rebuilding of the subaerial beach profile by swash activity throughout berm recovery.

Acknowledgments

This research was funded by the Australian Research Council [DP150101339]. The primary author was supported by an Australian Postgraduate Award and in part by the Coastal Processes and Responses Node Research Hub of the NSW Office of Environment and Heritage. Deployment of the lidar monitoring station was kindly assisted by Larry Paice, Daniel Howe, Michael Allis, Robert Thompson, Karina Taylor and Flight Deck apartment building. Wave and tide data was provided by Manly Hydraulics Laboratory on behalf of the NSW Office of Environment and Heritage (OEH). Nearshore wave modelling was undertaken by Thomas Mortlock, Macquarie University. Data for this study is available online on Dryad Digital Repository (https://doi.org/10.5061/dryad.774c492) and is titled *"Data from: Modes of berm and beachface recovery following storm reset: observations using a continuously scanning lidar"* doi:10.5061/dryad.774c492.

References

Austin, M. J., & Masselink, G. (2006). Observations of morphological change and sediment transport on a steep gravel beach. *Marine Geology, 229*(1–2), 59-77. doi:10.1016/j.margeo.2006.02.003

Baldock, T. E., Barnes, M. P., & Hughes, M. G. (2006). *Field observations of instantaneous cross-shore free surface profiles and flow depths in the swash zone*. Paper presented at the International Conference on Coastal Dynamics 2005, Barcelona, Spain.

Baldock, T. E., Weir, F., & Hughes, M. G. (2008). Morphodynamic evolution of a coastal lagoon entrance during swash overwash. *Geomorphology, 95*(3–4), 398-411. doi:10.1016/j.geomorph.2007.07.001

Bascom, W. N. (1954). *Characteristics of natural beaches*. Paper presented at the 4th Conference on Coastal Engineering, Chicago, United States. https://icce-ojs-tamu.tdl.org/icce/index.php/icce/article/view/1588

Blenkinsopp, C. E., Mole, M. A., Turner, I. L., & Peirson, W. L. (2010). Measurements of the time-varying free-surface profile across the swash zone obtained using an industrial LIDAR. *Coastal Engineering, 57*(11–12), 1059-1065. doi:10.1016/j.coastaleng.2010.07.001

Blenkinsopp, C. E., Turner, I. L., Masselink, G., & Russell, P. E. (2011). Swash zone sediment fluxes: Field observations. *Coastal Engineering, 58*(1), 28-44. doi:10.1016/j.coastaleng.2010.08.002

Brodie, K. L., Slocum, R. K., & McNinch, J. E. (2012). *New insights into the physical drivers of wave runup from a continuously operating terrestrial laser scanner.* Paper presented at the Oceans 2012, Hampton Roads, United States.

Burvingt, O., Masselink, G., Scott, T., Davidson, M., & Russell, P. (2018). Climate forcing of regionally-coherent extreme storm impact and recovery on embayed beaches. *Marine Geology, 401*, 112-128.

Castelle, B., Bujan, S., Ferreira, S., & Dodet, G. (2017). Foredune morphological changes and beach recovery from the extreme 2013/2014 winter at a high-energy sandy coast. *Marine Geology, 385*, 41-55. doi:10.1016/j.margeo.2016.12.006

CERC. (1984). *Shore Protection Manual*. Retrieved from Washington, D.C., United States:

Corbella, S., & Stretch, D. (2012). Shoreline recovery from storms on the east coast of Southern Africa. *Natural Hazards and Earth System Science, 12*(1), 11-22. doi:10.5194/nhess-12-11-2012

Couriel, E., Alley, K., & Modra, B. (2012). *OEH NSW Tidal Planes Analysis 1990–2010 Harmonic Analysis* (Report MHL2053). Retrieved from Sydney, Australia:

Davidson, M. A., Splinter, K. D., & Turner, I. L. (2013). A simple equilibrium model for predicting shoreline change. *Coastal Engineering, 73*, 191-202. doi:10.1016/j.coastaleng.2012.11.002

Dean, R. G. (1973). *Heuristic Models of Sand Transport in the Surf Zone*. Paper presented at the Conference on Engineering Dynamics in the Coastal Zone, Sydney, Australia.

DHI. (2014). *MIKE21 SW. Spectral Wave FM Module User Guide*. Retrieved from Hørsholm, Denmark:

Dubois, R. N. (1988). Seasonal changes in beach topography and beach volume in Delaware. *Marine Geology, 81*(1–4), 79-96. doi:10.1016/0025-3227(88)90019-9

Dodet, G., Castelle, B., Masselink, G., Scott, T., Davidson, M., Floc'h, F., et al. (2018). Beach recovery from extreme storm activity during the 2013–14 winter along the Atlantic coast of Europe. *Earth Surface Processes and Landforms*, *44*, 393–401. doi:10.1002/esp.4500

Frampton, A. P. R. (2010). A Review of Amenity Beach Management. *Journal of Coastal Research, 26*(6), 1112-1122. doi:10.2112/JCOASTRES-D-09-00008.1

Gourlay, M. R. (1968). *Beach and Dune Erosion Tests* (Report M935/M936). Retrieved from Delft, Netherlands:

Guedes, R. M. C., Bryan, K. R., Coco, G., & Holman, R. A. (2011). The effects of tides on swash statistics on an intermediate beach. *Journal of Geophysical Research: Oceans, 116*(C4), C04008. doi:10.1029/2010JC006660

Harley, M. D., Turner, I. T., Short, A. D. and Ranasinghe, R., (2011). A reevaluation of coastal embayment rotation: The dominance of cross-shore versus alongshore sediment transport processes, Collaroy-Narrabeen Beach, southeast Australia. *Journal of Geophysical Research: Earth Surface, 116(F4)*, F04033. doi: 10.1029/2011JF001989.

Harley, M. D., Turner, I. L., Kinsela, M. A., Middleton, J. H., Mumford, P. J., Splinter, K. D., et al. (2017). Extreme coastal erosion enhanced by anomalous extratropical storm wave direction. *Scientific Reports, 7*(1), 6033. doi:10.1038/s41598-017-05792-1

Harley, M. D., Turner, I. L., & Short, A. D. (2015). New insights into embayed beach rotation: The importance of wave exposure and cross-shore processes. *Journal of Geophysical Research: Earth Surface, 120*(8), 1470–1484. doi:10.1002/2014JF003390

Harley, M. D., Turner, I. L., Splinter, K. D., Phillips, M. S., & Simmons, J. A. (2016). Beach response to Australian East Coast Lows: A comparison between the 2007 and 2015 events, Narrabeen-Collaroy Beach. *Journal of Coastal Research, SI*(75), 388-392. doi:10.2112/SI75-078.1

Hine, A. C. (1979). Mechanisms of berm development and resulting beach growth along a barrier spit complex. *Sedimentology, 26*(3), 333-351. doi:10.1111/j.1365-3091.1979.tb00913.x

Holman, R. A. and Stanley, J. (2007) The history and technical capabilities of Argus. *Coastal Engineering, 54*(6-7), 477-491.

Houser, C., Wernette, P., Rentschlar, E., Jones, H., Hammond, B., & Trimble, S. (2015). Post-storm beach and dune recovery: Implications for barrier island resilience. *Geomorphology, 234*, 54-63. doi:10.1016/j.geomorph.2014.12.044

Jensen, S. G., Aagaard, T., Baldock, T. E., Kroon, A., & Hughes, M. (2009). Berm formation and dynamics on a gently sloping beach; the effect of water level and swash overtopping. *Earth Surface Processes and Landforms, 34*(11), 1533-1546. doi:10.1002/esp.1845

Katoh, K., & Yanagishima, S.-i. (1992). *Berm formation and berm erosion*. Paper presented at the International Conference on Coastal Engineering, Venice, Italy.

Kobayashi, N., & Jung, H. (2012). Beach Erosion and Recovery. *Journal of Waterway, Port, Coastal, and Ocean Engineering, 138*(6), 473-483. doi:10.1061/(ASCE)WW.1943-5460.0000147

Larson, M., & Kraus, N. C. (1989). *SBEACH: Numerical model for simulating storm-induced beach change- Report 1. Empirical foundation and model development* (CERC-89-9). Retrieved from Washington, D.C., United States:

Masselink, G., & Hughes, M. G. (2003). *Introduction to coastal processes and geomorphology* (1 ed.). London, United Kingdom: Hodder Arnold.

Mortlock, T. R., & Goodwin, I. D. (2016). Impacts of enhanced central Pacific ENSO on wave climate and headland-bay beach morphology. *Continental Shelf Research, 120*, 14-25. doi:10.1016/j.csr.2016.03.007

Morton, R. A., Paine, J. G., & Gibeaut, J. C. (1994). Stages and Durations of Post-Storm Beach Recovery, Southeastern Texas Coast, U.S.A. *Journal of Coastal Research, 10*(4), 884-908. doi:10.2307/4298283

Phillips, M. S., Harley, M. D., Turner, I. L., Splinter, K. D., & Cox, R. J. (2017). Shoreline recovery on wave-dominated sandy coastlines: the role of sandbar morphodynamics and nearshore wave parameters. *Marine Geology, 385*, 146-159. doi:10.1016/j.margeo.2017.01.005

Psuty, N. P. (1965). Beach-ridge development in Tabasco, Mexico. *Annals of the Association of American Geographers, 55*(1), 112-124. doi:10.1111/j.1467-8306.1965.tb00509.x

Puleo, J. A., & Torres-Freyermuth, A. (2016). The second international workshop on swash-zone processes. *Coastal Engineering, 115*, 1-7. doi:10.1016/j.coastaleng.2015.09.007

Revell, D. L., Dugan, J. E., & Hubbard, D. M. (2011). Physical and Ecological Responses of Sandy Beaches to the 1997–98 El Niño. *Journal of Coastal Research, 27*(4), 718-730. doi:10.2112/JCOASTRES-D-09-00179.1

Roelvink, D., Reniers, A., van Dongeren, A., van Thiel de Vries, J., McCall, R., & Lescinski, J. (2009). Modelling storm impacts on beaches, dunes and barrier islands. *Coastal Engineering, 56*(11–12), 1133-1152. doi:10.1016/j.coastaleng.2009.08.006

Roy, P. S., Thom, B. G., & Wright, L. D. (1980). Holocene sequences on an embayed high-energy coast: an evolutionary model. *Sedimentary Geology, 26*(1), 1-19. doi:10.1016/0037-0738(80)90003-2

Russell, P. E., Masselink, G., Blenkinsopp, C., & Turner, I. L. (2009). A Comparison of Berm Accretion in the Swash Zone on Sand and Gravel Beaches at the Timescale of Individual Waves. *Journal of Coastal Research, SP*(56), 1791-1795.

Scott, T., Masselink, G., O'Hare, T., Saulter, A., Poate, T., Russell, P., et al. (2016). The extreme 2013/2014 winter storms: Beach recovery along the southwest coast of England. *Marine Geology, 382*, 224-241. doi:10.1016/j.margeo.2016.10.011

Shand, T., Goodwin, I., Mole, M., Carley, J., Coghlan, I., Harley, M., & Peirson, W. (2010). *NSW coastal inundation hazard study: coastal storms and extreme waves* (Report 16). Retrieved from Sydney, Australia:

Short, A. D., & Trenaman, N. L. (1992). Wave climate of the Sydney region, an energetic and highly variable ocean wave regime. *Marine and Freshwater Research, 43*(4), 765-791. doi:10.1071/MF9920765

Splinter, K., Harley, M., & Turner, I. (2018). Remote Sensing Is Changing Our View of the Coast: Insights from 40 Years of Monitoring at Narrabeen-Collaroy, Australia. *Remote Sensing, 10*(11), 1744.

Thom, B. G. (1984). Transgressive and regressive stratigraphies of coastal sand barriers in southeast Australia. *Marine Geology, 56*(1), 137-158. doi:10.1016/0025-3227(84)90010-0

Turner, I. L., Harley, M. D., Short, A. D., Simmons, J. A., Bracs, M. A., Phillips, M. S., & Splinter, K. D. (2016). A multi-decade dataset of monthly beach profile surveys and inshore wave forcing at Narrabeen, Australia. *Scientific Data, 3*, 160024. doi:10.1038/sdata.2016.24

Turner, I. L., Russell, P. E., & Butt, T. (2008). Measurement of wave-by-wave bed-levels in the swash zone. *Coastal Engineering, 55*(12), 1237-1242. doi:10.1016/j.coastaleng.2008.09.009

Weir, F. M., Hughes, M. G., & Baldock, T. E. (2006). Beach face and berm morphodynamics fronting a coastal lagoon. *Geomorphology, 82*(3–4), 331-346. doi:10.1016/j.geomorph.2006.05.015

Wright, L. D., & Short, A. D. (1984). Morphodynamic variability of surf zones and beaches: A synthesis. *Marine Geology, 56*(1–4), 93-118. doi:10.1016/0025-3227(84)90008-2

Yu, F., Switzer, A. D., Lau, A. Y. A., Yeung, H. Y. E., Chik, S. W., Chiu, H. C., et al. (2013). A comparison of the post-storm recovery of two sandy beaches on Hong Kong Island, southern China. *Quaternary International, 304*, 163-175. doi:10.1016/j.quaint.2013.04.002

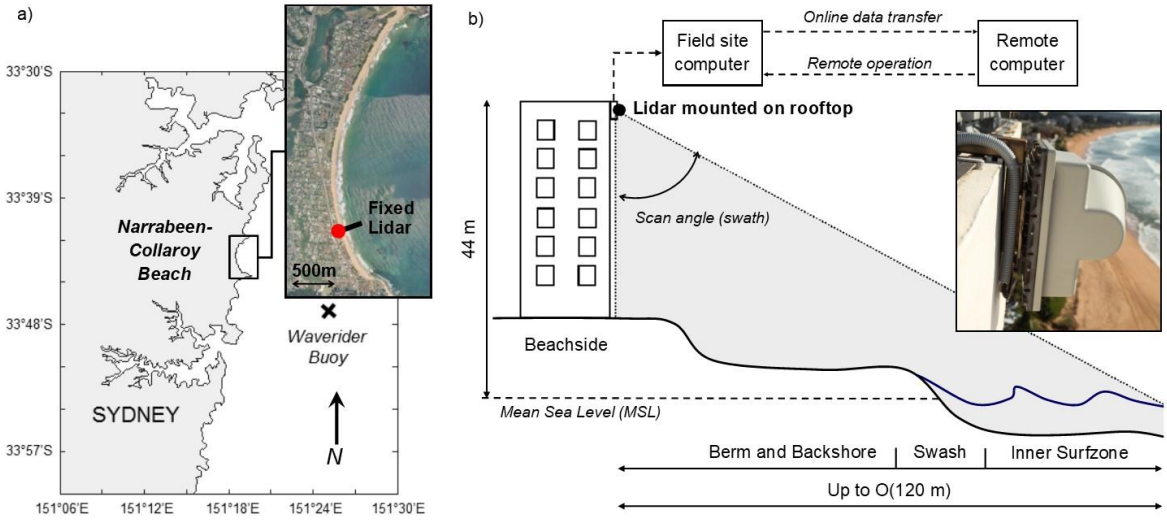

Figure 1: a) Study site location Narrabeen-Collaroy Beach situated on SE Australian coastline near Sydney. b) Schematic and photograph of fixed lidar monitoring system setup with instrument mounted on rooftop of beachside apartment building.

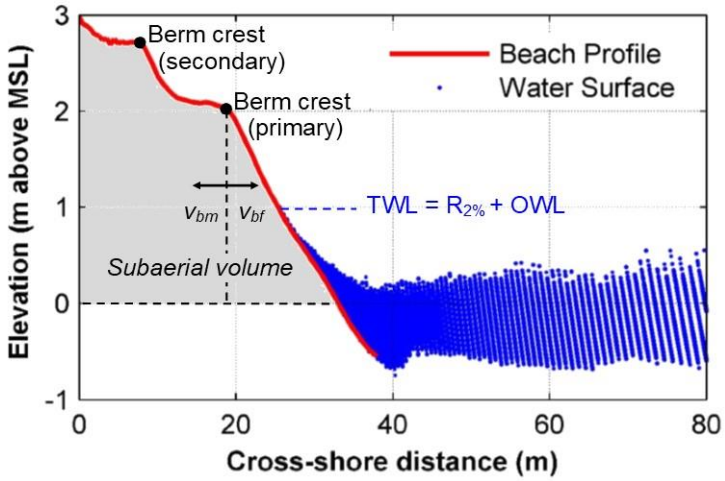

Figure 2: Example of profile, swash and surf zone water surface lidar measurements during a 30 min scan at low tide (10:47 - 11:17, 29th May 2015). Also noted are positions of the primary (most seaward) and secondary (landward) berm crests as well as the TWL.

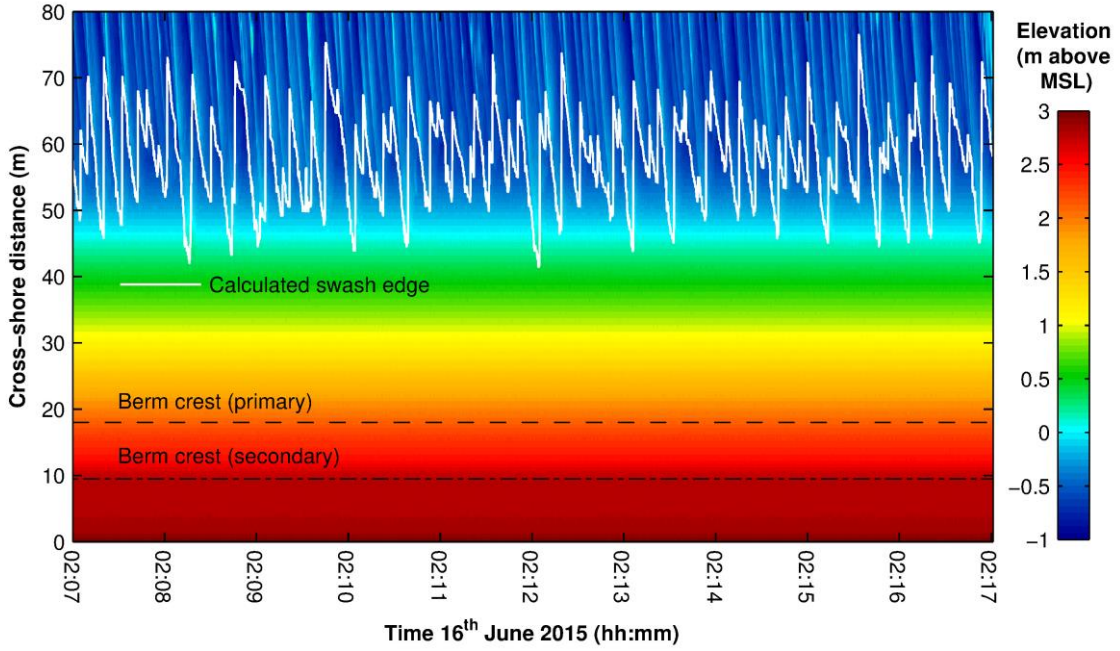

Figure 3: Example time series of subaerial beach profile and water surface lidar measurements collected over a 10-minute period on 16th June 2015. The positions of the extracted swash edge and berm crests are shown. Note the capability of the lidar to collect profile, swash and inner surf zone data outside of daylight hours, providing continuous, high temporal resolution monitoring over extending periods of time.

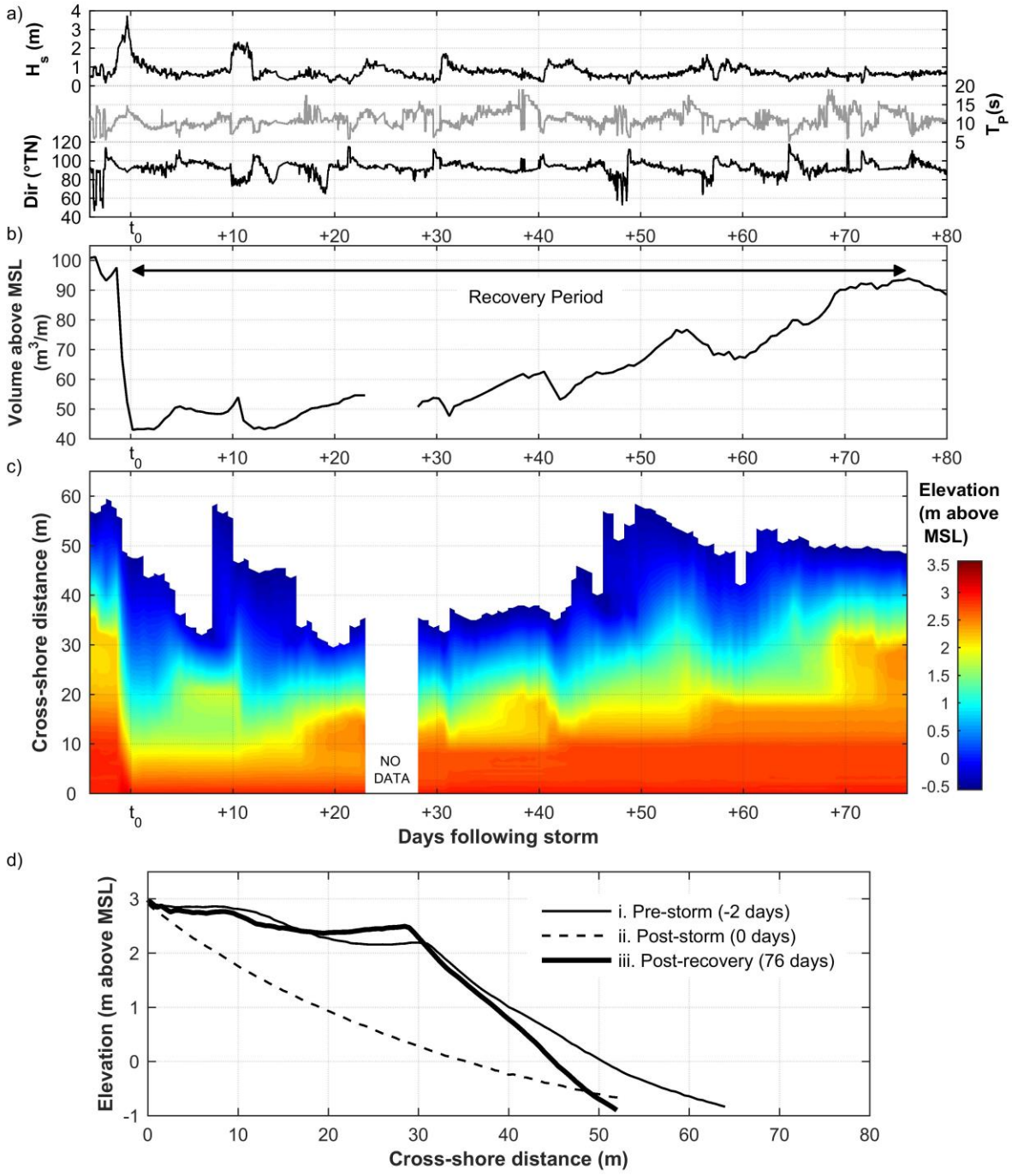

Figure 4: Beach recovery following 20 - 22 April 2015 storm. Time series during the storm and subsequent recovery period are shown for a) hourly measured nearshore significant wave height (H_s) peak wave period (T_p) and wave direction at the 10 m depth contour, b) tide-by-tide measurements of subaerial beach sediment volume, and c) tide-by-tide beach profile evolution. d) Beach profiles immediately before the storm (pre-storm), immediately after the storm (post-storm) and at the end of the recovery period (post-recovery). No data was collected between days 23 and 28 due to a technical issue with the field site computer.

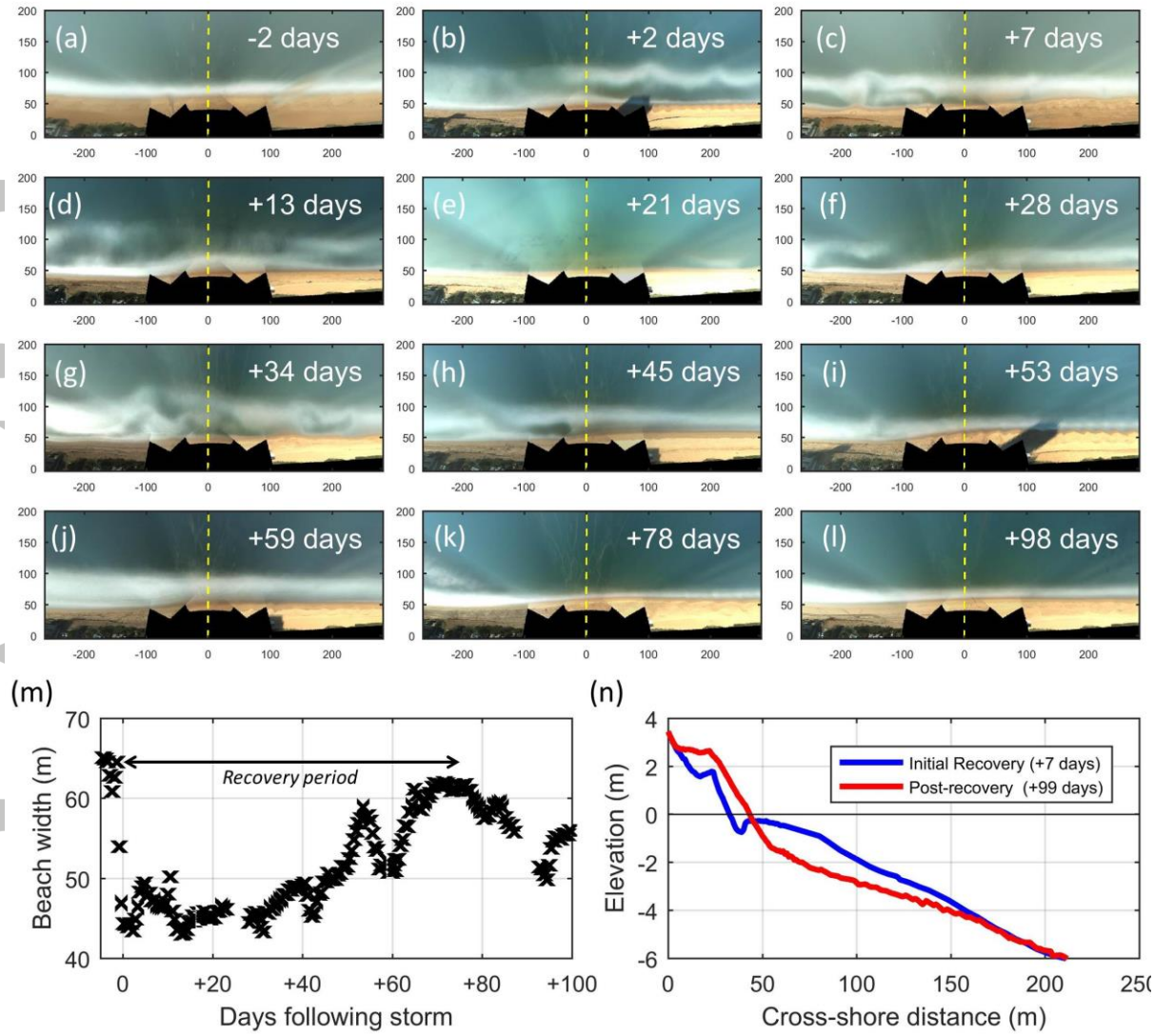

Figure 5. Sequence of mid-tide planview timex images from the Narrabeen-Collaroy coastal imaging station (dash line indicates cross-shore profile of the lidar) showing the temporal evolution of the nearshore bathymetry and beach during this recovery period. Nearshore wave breaking patterns show examples of 2DH bathymetry (e.g. +34 days), alongshore uniform bars (+45; +59 days) and reflective conditions (+53, +78, +98 days). Beach cusps are present in the subaerial beach at +2, +7, +53 and +78 days. Bar-welding events occur between days +45 to +53 and +59 to +78. (m) measured beach width from the fixed lidar during this recovery period. (n) post-storm surveys at the lidar profile undertaken at +7 and +99 days using RTK-GPS and jetski echosounder.

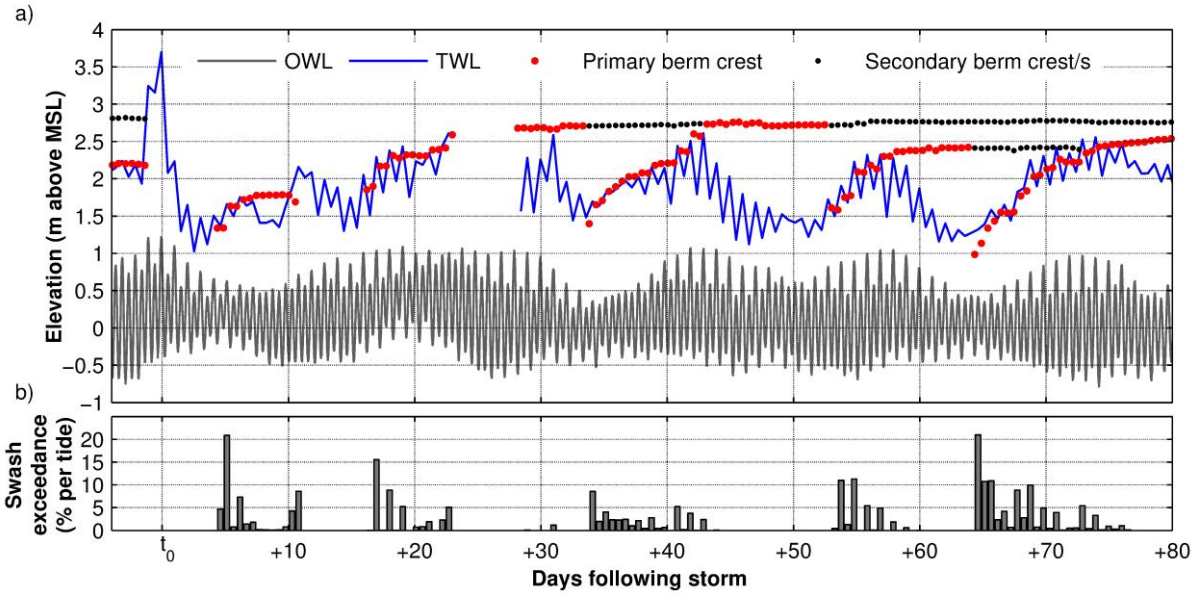

Figure 6: a) Elevation time series of ocean water levels (OWL), total water level (*TWL*), primary (most seaward) berm crest and secondary (landward, inactive) berm crests throughout the recovery period. Patterns of berm crest formation and vertical growth are noted with neap-spring variations in total water levels. b) The percentage of wave runup events exceeding the berm crest for each tidal cycle (approx. 12 h period) throughout recovery.

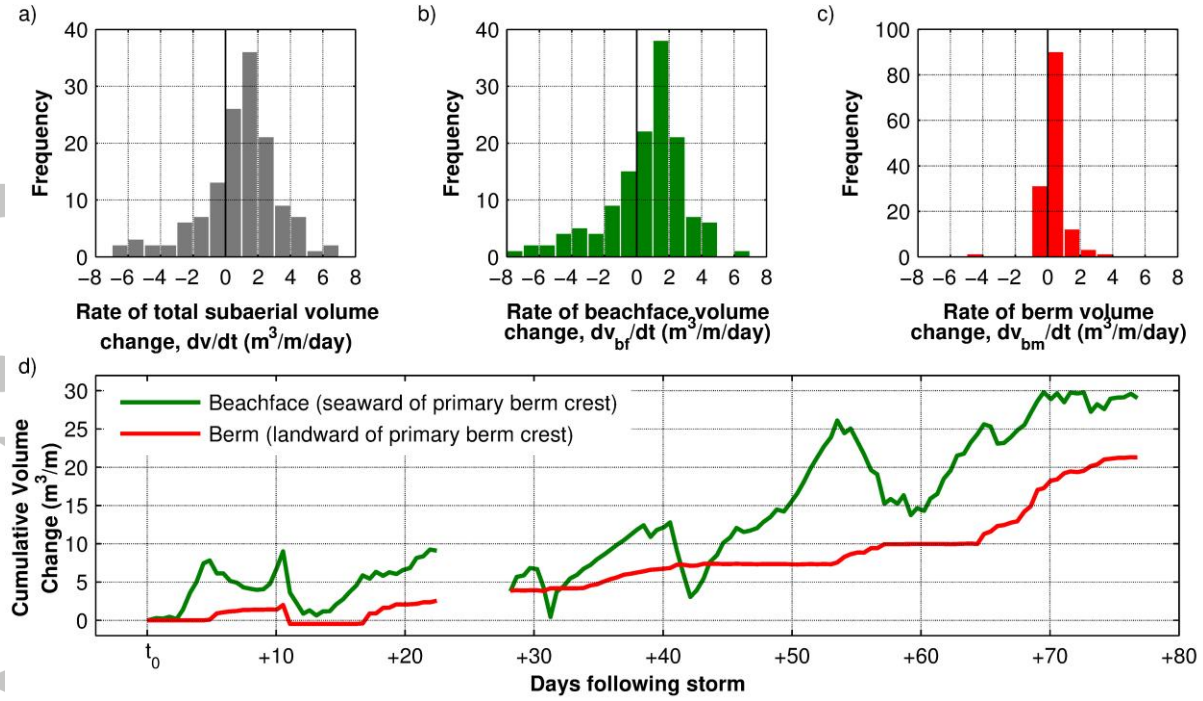

Figure 7: Histograms showing the distribution of tide-by-tide rates of volume change for regions of the a) total subaerial beach, b) beachface (seaward of the primary berm crest) and c) berm (landward of the primary berm crest). Note change in y-axis scaling d) Cumulative volume changes on the beachface and berm during post-storm recovery.

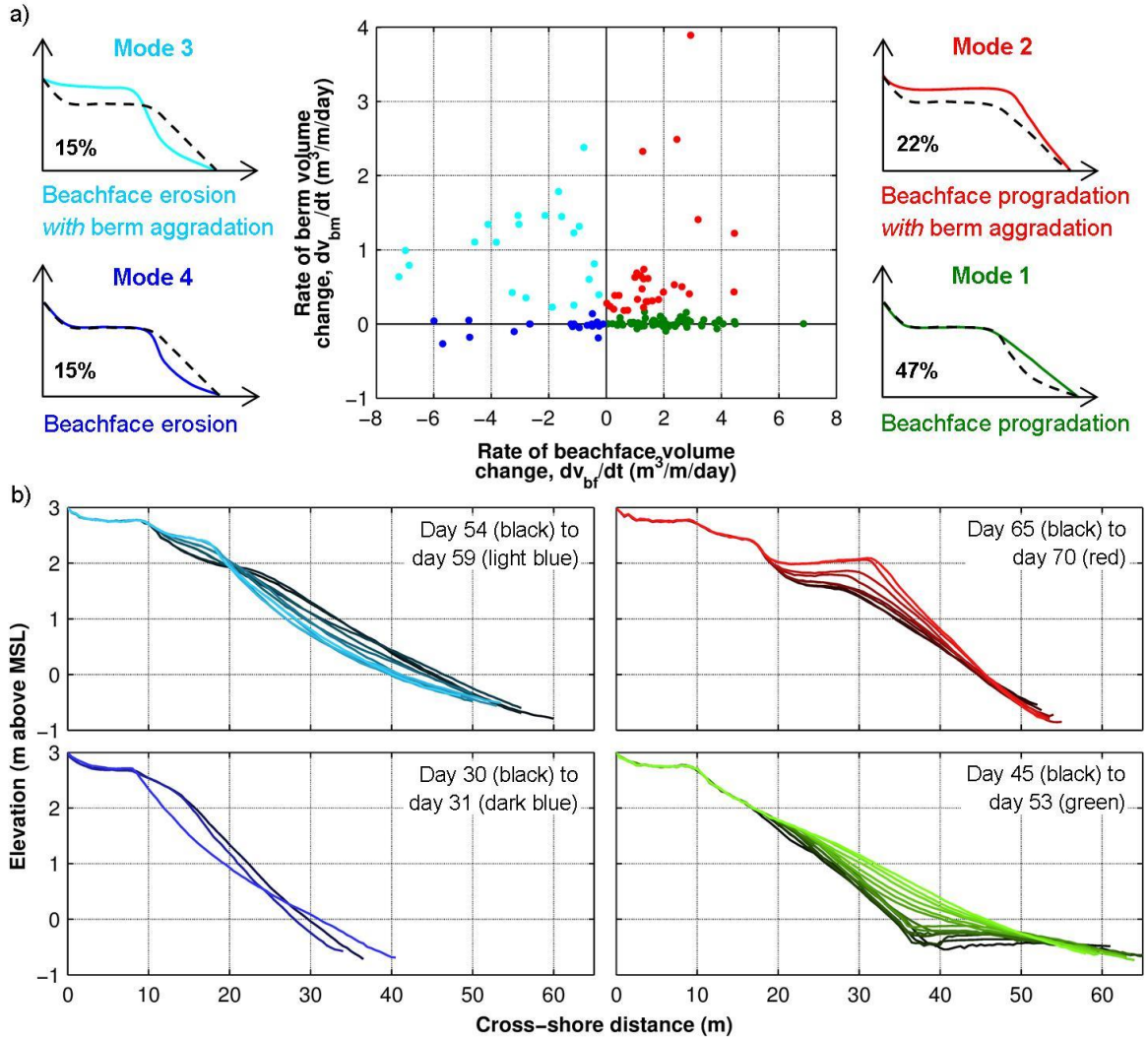

Figure 8: a) Classification of four principal modes of subaerial beach profile variability throughout berm recovery based on tide-by-tide lidar measurements. Corresponding profile changes are illustrated and labelled with the dashed profile indicating initial conditions. Percentages of observations for each mode are also shown. b) Example phases during recovery showing profile development for each mode.

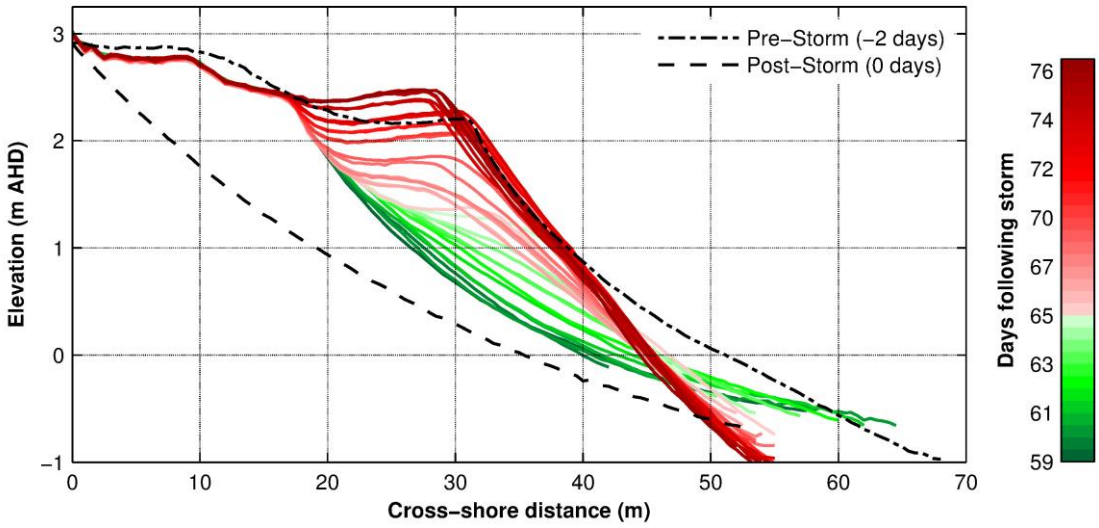

Figure 9: Tide-by-tide beach profile changes during the final 17 days of berm recovery. Beachface progradation (mode 1) is shown in green from day 59 to 65 leading to the formation of a neap berm. This is followed by significant berm aggradation (predominantly mode 2 with some mode 3) shown in red from day 65 to 76.

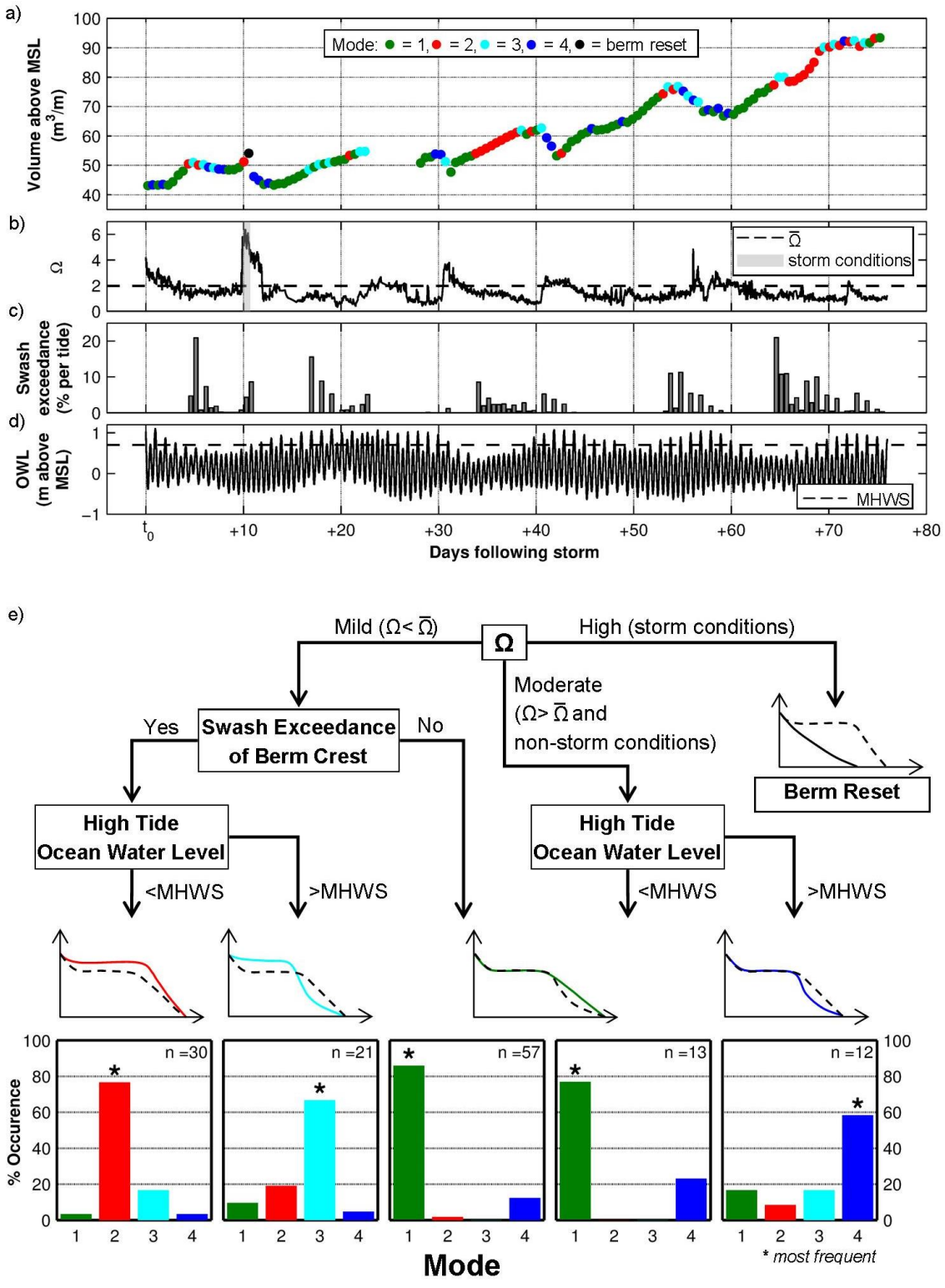

Figure 10: Time series (12-hourly) throughout recovery of a) principal modes of berm recovery, b) nearshore Ω, c) swash exceedance of the berm crest per tidal cycle and d) ocean water levels. The decision tree in e) shows hydrodynamic conditions distinguishing the occurrence of each mode. $\bar{\Omega}$ refers to the 12-year site mean nearshore dimensionless fall velocity (≈ 2.0). Storm conditions refer to significant wave heights above the 5% exceedance level for a minimum duration of one tidal cycle (≈12h period), during which Ω was observed to exceed the value of 4. MHWS refers to mean high water springs (≈ 0.7 m above MSL). The total number of observed responses for each tidal cycle during the recovery period is given by n.